Materials Science Research International, Vol.6, No.2 pp.65-73 (2000)

Review paper

Application of Micromechanics to Modeling Compressive Failure of Rock

Yoshiaki OKUI* and Hideyuki HORII**

*Department of Civil and Environmental Engineering, Saitama University, Shimo-ohkubo 255, Urawa, 338-8570, Japan
**Department of Civil Engineering, University of Tokyo, Bunkyo-ku, Tokyo, 113-8654, Japan

Abstract: This article presents a review of the research work related to the micromechanical modeling of behavior of hard rock under compression. To this end, it initially provides observed macroscopic behavior of compressive rock for both time-independent and -dependent cases. It proceeds with a review of microscopic observations of rock failure including recent techniques in rock experiments. Crack growth laws in rock for both short- and long-term loading are next reviewed. Finally, micromechanical models employed in literatures and associated continuum theories based on micromechanics are introduced.

Key words: *Micromechanics, Rock mechanics, Fracture mechanics, Subcritical crack growth, Localization of deformation, Continuum model, Damage mechanics*

1. INTRODUCTION

In the last two decades, a number of studies on microstructure in rock have been done. One of the reasons for this activity is the rapid development both of experimental equipment for the mechanical testing of rocks, and of observation devices, such as optical and electron microscopes, transducers for acoustic emission, and so on. Another more essential reason is that microstructure itself is attractive for a wide range of researchers in the fields of mechanics, geology, geophysics, mechanical engineering, and civil engineering. Microcracks, a governing microscopic event responsible for inelastic behavior and the eventual macroscopic fracture of rocks, are easier to observe than dislocations in metal plasticity. Accordingly, there is a clear motivation to explain the varied behavior of rock in terms of microcrack growth, configuration, interaction, and statistical distribution. Furthermore, the development of fracture mechanics for metals in 1960's and its successful application to nonmetals in 1970's also supports researchers' interest in microcracks.

With a view to motivating further developments in the subject, this paper presents a review of research related to the application of micromechanics to the mechanical behavior of hard rock. Attention is limited to the quasi-static response of hard rock under macroscopically compressive stresses. The selection of topics reflects the authors' interests. Research relating to sedimentary soft rock and jointed rock masses is excluded.

Chapter 2 will summarize the typical behavior of hard rocks observed in uniaxial and multiaxial tests for both short and long-term loading. In Chapter 3, experimental observations on microscopic events in compressive rock will be reported. Chapter 4 will introduce crack growth laws and associated studies on hard rocks. In Chapter 5, micromechanical models employed in previous studies will be illustrated. Finally, continuum theories based on micromechanics will be reviewed in Chapter 6.

2. MACROSCOPIC BEHAVIOR

One of the major objectives of micromechanics is to explain macroscopic behavior on the basis of microscopic events. Before introducing microscopic events in rock under compression, typical macroscopic behavior which has been observed and reported in many papers will be described in this chapter.

2.1. Short-term Behavior

The triaxial compression test of rock can be traced to the pioneering work by von Karman in 1911; see [1] for a historical review of rock testing methods. Since then, it has been widely accepted the compressive strengths and failure modes of rock depend on confining pressure. The determination of the deformation and strength of rock under compressive stress has been a problem of great interest for geology, seismology, mining as well as the oil industry. In particular, since the end of the 1950's a great deal of triaxial compression test data has been reported [2–6]. For instance, one of the earliest papers in 1957 [2] on triaxial tests of sedimental rocks presented the effects of confining pressure up to 200 MPa on its strength.

In 1966, Brace et al. [4] reported triaxial compression data of Westerly granite with a confining pressure of up to 800 MPa. Figure 1 shows the triaxial compression data by Brace et al. together with

Received March 13, 2000
Accepted May 2, 2000

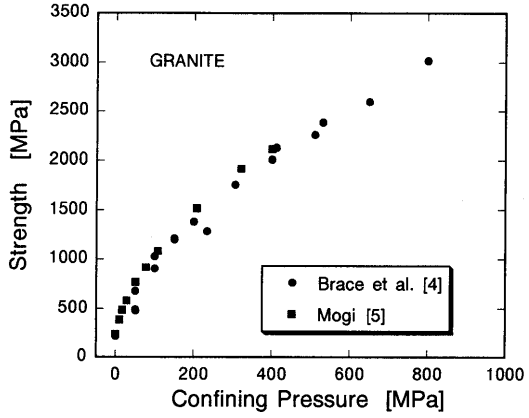

Fig.1. Compressive fracture strength of Westerly granite.

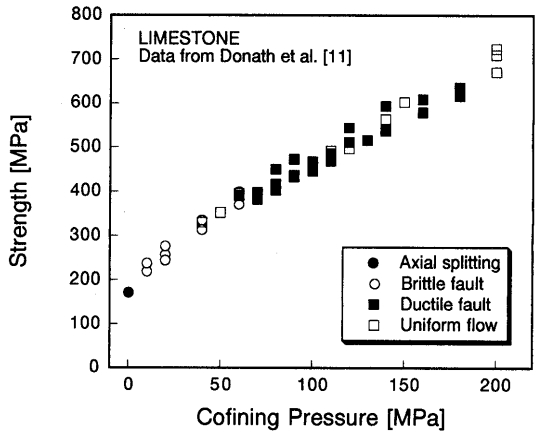

Fig.2. Compressive fracture strength of limestone with macroscopic failure mode, Failure mode changes from Axial splitting to Brittle fault, to Ductile fault, and to Uniform flow.

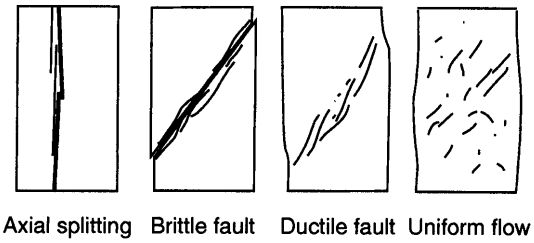

Fig.3. Sketch of macroscopic failure mode in triaxial compression tests by Donath et al. [11]. Failure modes corresponds to the legends in Fig. 2 .

Mogi [5], which illustrates the dependence of compressive strengths on confining pressure. Based on this experimental data, empirical formulae for compressive strength, such as the Mohr envelope, were proposed; see [7,8] and a review article [9].

At the same time, the transition of macroscopic failure modes with increasing confining pressure has attracted considerable attention [6, 10, 11]. In a lot of hard rock, the macroscopic failure modes change from brittle to ductile deformation with increasing confining pressure, and accordingly this transition is referred to as the brittle-ductile transition. As another clear example, Fig. 2 demonstrates the effects of confining pressure on the failure modes and strengths of limestone reported by Donath et al. [11]. The failure mode of limestone changes from axial splitting to brittle faulting, to ductile faulting, and then to uniform flow with increasing confining pressure and strain; see, Fig. 3 for sketches of the failure modes.

2.2. Long-term Behavior

The long-term behavior of rocks under constant stress is of great interest as well, because stresses within the earth's crust generally do not vary rapidly. In addition, it is also very important, from an engineering view point, to ensure the long-term stability of large underground spaces such as caverns for power stations, and storage facilities [12].

For the long-term behavior of rock, since the authors' choice of articles is somewhat arbitrarily restricted, it might be useful to recall two books [13] for testing methods and data and [14] for testing methods and results and some proposed phenomenological constitutive models.

Rock at low temperatures under a constant stress close to the short-term strength will rupture in a brittle manner after a certain length of time, and this type of loading test is called a creep test; see also [15–18]. The time to rupture depends on the applied stress. If the applied stress is close to the short-term strength, then the time to rupture becomes short. The strain history under constant stress is called the creep curve. In general, a creep curve can be divided into three stages, namely primary, secondary and tertiary creep, as shown in Fig. 4. Primary creep is characterized by a rapid increase in strain just after loading; in secondary creep, the strain rate is slow and constant; tertiary creep is the onset of instability leading to eventual fracture.

A series of systematic creep tests was conducted by Kranz et al. [19–21]. They showed the dependence of the time to failure on confining pressure and applied stress difference in a creep test [21] as shown in Fig. 5. In this figure, σ_1 and p_c are the applied axial stress and the confining pressure in a creep test, respectively; and $(\sigma_1 - p_c)_{\max}$ stands for the stress difference in the short-term test with the same confining pressure as the corresponding creep tests. If $(\sigma_1 - p_c)/(\sigma_1 - p_c)_{\max} = 1$, then the specimen fails immediately. It is seen that the time to failure increases with any decrease in the normalized stress difference,

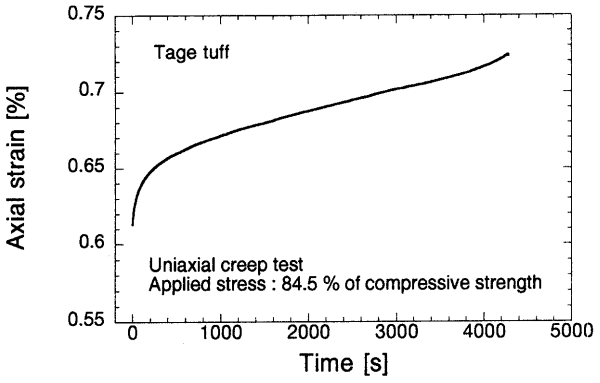

Fig.4. Creep curve of Taya tuff. Uniaxial creep test. Courtesy of Dr. Yamabe of Saitama Univ.

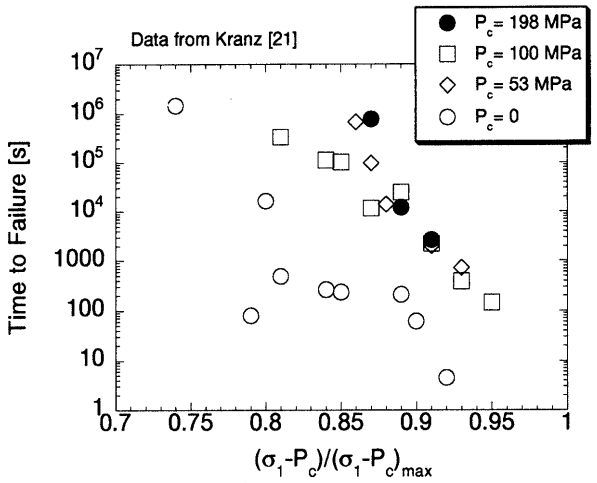

Fig.5. Effect of confining pressure p_c and stress difference $(\sigma_1 - p_c)$ on time to fracture in creep tests of Barre granite. (σ_1: maximum compressive stress; $(\sigma_1 - p_c)_{max}$: stress difference in the short-term test).

and the confining pressure fosters this tendency.

Kranz et al. also reported the failure mode in creep tests. Excepting uniaxial creep tests, faulting similar to that in short-term tests was observed in creep tests as well, and a failure plane in a creep test was inclined with respect to the direction of maximum compression. The effect of confining pressure on the fracture angle that is the angle from the maximum compressive direction to the eventual failure plane is shown in Fig. 6 for creep tests by Kranz [21] together with conventional short-term compression tests. It is seen that the fracture angle increases with any increase in the confining pressure, and the tendency of the fracture angle in creep tests is similar to that in short-term tests.

Another important aspect of time-dependent behavior is the effect of environmental conditions such as temperature, existence of water [22]. Lajitai et al. [23] conducted creep tests under three different environmental conditions. It was shown that the long-term strength decreases when water is introduced.

3. MICROSCOPIC BEHAVIOR

Experimental observations on microscopic events in compressive rocks are sketched in this chapter. A earlier review article [24] presents more detailed description on studies about microcracks in rock including kinematics, population statics, and observation techniques.

Observation of microstructure in compressive rock was begun with optical microscopes; see [25,26]. Since the beginning of the 1970's, quantitative information on microstructure, such as crack density and orientation of microcracks has been reported [27–29]. Wawersik and Brace [27] investigated the relationship between the crack density at the maximum stress state and confining pressure. They reported that the crack density in Westerly granite at the maximum stress state increases sharply with confining pressure and reaches an approximately constant level about a confining pressure of p_c =20 MPa. For crack orientation, the density of cracks with low angle (< 5°) with respect to the maximum compression is greatest when p_c < 30 MPa, while the high angle density (> 30°), in turn increases with confining pressure. Furthermore, Hallbauer et al. [28] investigated the process of faulting, and reported density maps of microcracks at several points of a stress–strain curve of quartzite. It was shown that microcracking is mainly intra-granular and parallel to the direction of the maximum principal stress, and that microcracks in high density areas eventually coalesce to form the macroscopic fracture.

At almost the same time as the above qualitative reports with optical microscopies, the scanning electron microscope (SEM) has been utilized to observe the microstructure of rocks. Timur et al. [30] investigated pore structure in unstressed samples of sandstone, limestone, dolomite, and granite. Tapponnier and Brace [31] used samples with a surface polished by ion thinning to investigate stress-induced microcracks and pores in Westerly granite with a resolution of 10^{-6} cm. They presented some sketches of stress-induced microcracks under compression as shown in Fig. 7.

Sprunt and Brace [32] reported frequency distribution of crack and cavity lengths, aspect ratios, and orientation of unstressed and stressed samples of Westerly granite. They reported that the stress-induced cracks are sharp-ended, long, and narrow, while most initial defects are low-aspect-ratio cavities with blunt or rounded ends. Hadley [33] investigated crack and pore geometries in virgin and stressed Westerly granite with SEM. A remarkable point of her work is that she set sample areas (about 2 cm^2) for each specimen,

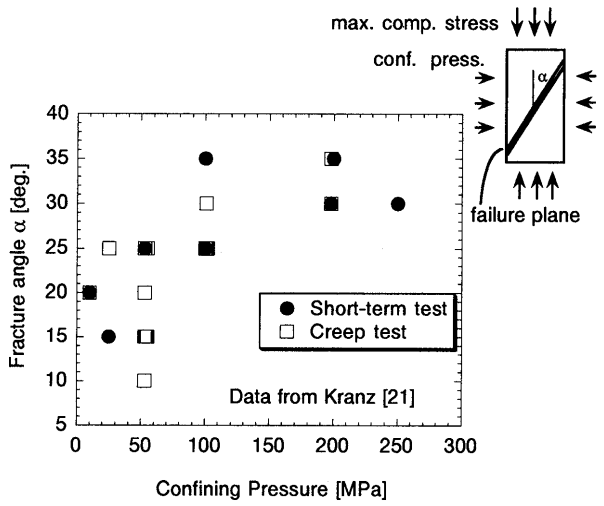

Fig.6. Fracture angle α of Barre granite in creep tests and short-term tests. Fracture angle is defined as the angle from the direction of the maximum compressive stress to the failure plane direction.

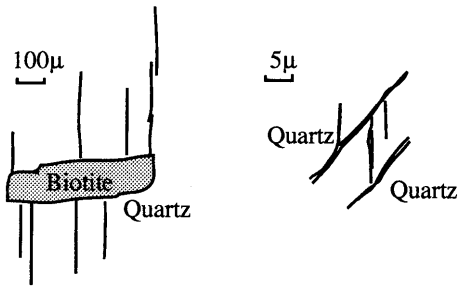

Fig.7. Sketch of stress-induced cracks. Max. compressive direction is vertical direction, and confining pressure is horizontal direction. After Tapponnier and Brace [31].

and measured lengths, widths, and orientations of all cracks and pores visible in the areas. In previous SEM observations, (e.g. [32]) a random sample of 80 cavities was chosen from the SEM observations to report the frequency distribution of crack lengths. Such an approach may not represent the averaged nature of microcracks as an example.

Kranz [20] studied crack growth during creep for Barre granite with SEM, and determined crack lengths and density, and the preferred orientation of microcracks at several stages in creep tests. It was shown that microstructure during creep is the same as that in short-term loading tests. Most cracks are parallel to the direction of maximum compressive stress. These cracks grow stably with time, and in the tertiary creep, localization and succeeding coalescence of microcracks eventually results in faults. Kranz [34] also directly observed crack-crack and crack-pore systems in stressed granite to investigate interaction effect on stress-induced crack growth; see also [35].

The process of microcracking localization in both short-term and creep tests is also observed with acoustic emission (AE); see early application of AE to rock failure [36–38], and a review in [39]. Yanagidani et al. [40] evaluated locations of AE hypocenters during creep of Oshima granite under uniaxial compression. They reported that, when loading up to a specific creep load level, AE locations were randomly distributed throughout a specimen. However, in primary creep, AE events formed volumetric concentrations. Recently, Lockner et al. [41, 42] showed a close correspondence between AE localized regions and eventual faulting planes in short-term tests. Furthermore they utilized the AE rate, which is the number of AE events per unit time, to control the applied load.

In recent rock experiments, Moore and Lockner [43] employed image analysis techniques to investigate microcracking near a laboratory shear fracture in a triaxial compression specimen of Westerly granite. Osada et al. [44, 45] used a replica method with the image analysis to quantify crack geometry data. Real-time SEM observation of fracture process of rocks was reported by Zhao et al. [46]. Transmission electron microscopes (TEM) have also been used to study microcracks in rocks [47]. More recently, non-destructive monitoring methods, such as X-ray CT scanning [48] and tomographic images of P-wave velocity [49] have been used.

4. CRACK GROWTH LAWS

As seen in the previous chapter, the nucleation, growth, and coalescence of microcracks is a dominant mechanism of the inelastic deformation and failure of brittle rock. In many cases, linear elastic fracture mechanics (LEFM) is employed as a microcrack growth criterion [50].

For short-term loading, as an example, the crack growth criterion based on LEFM can be written in terms of the mode I stress intensity factor K_{I} and the fracture toughness K_{Ic}:

$$\begin{cases} K_{\mathrm{I}} = K_{\mathrm{Ic}} & \text{growth.} \\ K_{\mathrm{I}} < K_{\mathrm{Ic}} & \text{no growth.} \end{cases} \tag{1}$$

At present LEFM parameters, such as fracture toughness, are recognized as one of the standard material parameters for brittle rock [51, 52]. Accordingly, a standard method to determine the fracture toughness has been recommended by the International Society for Rock Mechanics (ISRM) [53].

For long-term loading, slow and stable crack growth can occur, even though the stress intensity factor is substantially lower than its critical value, namely the fracture toughness. This phenomenon is known as subcritical crack growth [54–57]. Crack velocities

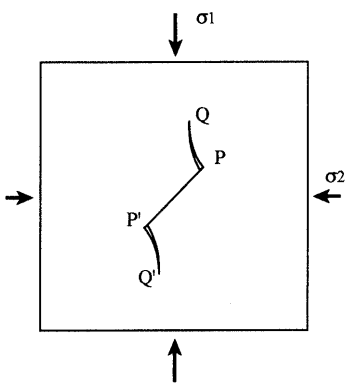

Fig.8. Sliding crack model: model of flaw under compression; PP': Initial angled crack; PQ and P'Q':Tension crack.

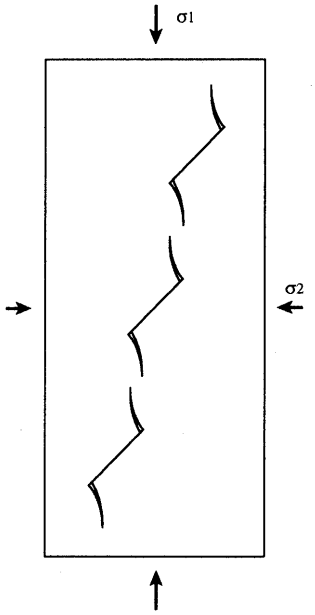

Fig.9. Echlon array of sliding cracks.

from 10^{-3} to 10^{-9} m/s are commonly measured in crack velocity tests for granitic rock [58]. The most often cited mechanism of subcritical crack growth is stress corrosion cracking; see an extensive review by Atkinson [59], and Atkinson and Meredith [60]. From crack velocity tests for rock, the relationship between the stress intensity factor K_I and the crack velocity v in the subcritical crack growth is most commonly expressed by a power law:

$$v = v_0(K_I/K_0)^n, \tag{2}$$

where v_0 is the crack velocity at $K_I = K_0$; v_0 and n are constants depending on the kind of rock and environmental conditions. The parameter n is known as the subcritical crack growth index, ranging from 30 to 50 for Westerly granite, as an example.

Environmental effects on subcritical crack growth are substantial. Meredith and Atkinson [61] conducted crack velocity tests using double torsion specimens in an environmental chamber to investigate temperature and water vapor pressure effects. Lajtai et al. [23] also conducted crack velocity tests as well as creep tests and short-term fracture tests under three different environmental conditions. They reported that the effect of water and temperature on the long-term strength and crack velocity in subcritical crack growth is more significant than that on the short-term strength.

These LEFM crack extension laws for both short- and long-term loading are utilized in the micromechanics of rock. That aspect will be explained in the next chapter.

For macrocrack growth, sometimes non-LEFM is employed. In order to apply LEFM, the inelastic region around microcrack tips must be small compared with other specimen dimensions (the small scale yielding condition). In polycrystalline rocks, it is reported that this inelastic region, called the process zone, consists of a cluster of microcracks [43, 62]. When the small scale yielding condition is violated, nonlinear fracture mechanics parameters, such as the J integral [63], can also be used as crack extension criteria. However, since non-LEFM parameters are mainly applied to the growth of macrocracks rather than microcracks, a review of non-LEFM parameters is omitted here.

5. MICROMECHANICAL MODEL

Probably, the most popular micromechanical model to represent cracks under compression is the so-called sliding crack model proposed by Brace and Bombolakis [64]; see Fig. 8. This sliding crack model consists of the initial crack-like slit PP' and the tension wing cracks PQ and P'Q'. The initial slit is inclined with respect to the direction of the maximum compressive stress σ_1. The surfaces of the initial slit come into contact with each other due to the compressive principle stresses σ_1 and σ_2. The frictional sliding on the initial slit results in the tension cracks PQ and P'Q'. Brace and Bombolakis [64] used photo elastic material and glass to investigate crack growth from the initial slit. They showed that tension cracks can grow stably and become parallel to the direction of the maximum compressive stress as the axial compressive stress increases. Furthermore, they described the relation between this experiment and shear fault in rock, and showed that the wing cracks in echelon arrays shown in Fig. 9 start to grow at a much smaller applied stress than that required for a single and isolated crack.

Nemat-Nasser and Horii [65] and Horii and Nemat-Nasser [66, 67] analyzed the response of a single sliding crack in a homogeneous medium under far-field

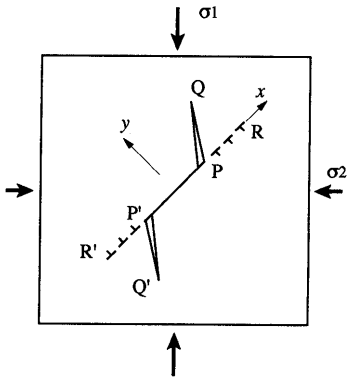

Fig.10. Sliding crack model with plastic zones PR and P'R'. From Horii and Nemat-Nasser [68].

compressive stresses. The boundary conditions on the initial slit PP' in Fig. 8 are

$$u_y^+ = u_y^-, \quad \tau_{xy}^+ = \tau_{xy}^- = -\tau_c + \mu\sigma_y, \tag{3}$$

where τ_c is the cohesive stress and μ is the friction coefficient. Superscripts + and − denote quantities on the upper and lower surfaces, respectively; subscripts x and y stand for quantities associated with parallel and normal directions to the initial slit, respectively. u_y is the displacement normal to the slit surface, τ_{xy} and σ_{yy} are the shear and normal stresses. Equation (1) was used as a crack growth law for tension cracks. They solved the problems numerically and conducted a series of model experiments to investigate the effect of confining pressure on macroscopic failure modes. In addition, they analyzed the response of Echelon arrays of shear cracks to investigate shear faulting.

Furthermore, Horii and Nemat-Nasser [68] used the model shown in Fig. 10 to estimate the brittle-ductile transition analytically. In this model, colinear plastic slips PR and P'R' are considered in addition to the shear crack model. The boundary conditions on the initial slit PP' in Fig. 8 were

$$u_y^+ = u_y^-, \quad \tau_{xy} = -\tau_Y, \tag{4}$$

where τ_Y is the yield stress in shear. The stresses at the ends of the plastic zones must be bounded. This condition requires that the mode II stress intensity factor at R and R' is zero:

$$K_{\mathrm{II}} = 0. \tag{5}$$

By comparing the plastic zone length PR with the maximum tension crack length PQ, and examining whether they grow in a stable or unstable manner, Horii and Nemat-Nasser made a brittle-ductile diagram.

Lockner [18] also used the sliding crack model to explain the mechanism of transition from the primary creep to the secondary creep. He employed a time-dependent crack growth law like Eq. (2).

Ashby et al. [69] employed the sliding crack model to examine the conditions under which an array of sliding cracks interact by using an approximate analytical theory as well as model experiments. Furthermore, Ashby and Sammis [70] developed a simpler damage model based on the interacting sliding crack models to predict the failure surface that defines macroscopic fracture in terms of stresses. However, these studies did not mention the stress-strain relationship. Continuum models based on micromechanics including the stress-strain relationship will be reviewed in the next chapter.

6. MICROMECHANICS-BASED CONTINUUM THEORY

Table 1 contains a summary of the selected publications describing micromechanics-based continuum models for rock under compression. Studies on more general mechanics associated with brittle cracked bodies have been reviewed by Kachanov [71] and by Nemat-Nasser and Hori [72] for overall properties, and by Krajcinovic [73] for damage mechanics. This kind of work is thus not included here.

Moss and Gupta [74] proposed a micromechanical constitutive model based on the response of sliding cracks and elliptic cracks. They considered strains due to elliptic crack opening as well as frictional sliding on initial angled crack and tension crack growth. This elliptic crack response represents the nonlinear elastic behavior of rock at small compressive stresses before frictional sliding and tension crack growth become dominant.

Kachanov [75, 76] considered frictional sliding on penny-shape cracks accompanied by the growth of flat circular cracks as a secondary tensile crack at the tip of the sliding crack. The macroscopic stress–strain relationship was derived from the average stress–strain relationship over the cracked medium. The strain caused by microcracks is given in terms of the displacement gaps $[\boldsymbol{u}]$ on the crack surfaces:

$$\boldsymbol{\epsilon}_c = \frac{1}{2V_e}\int_S ([\boldsymbol{u}] \otimes \boldsymbol{n} + \boldsymbol{n} \otimes [\boldsymbol{u}])ds, \tag{6}$$

where $\boldsymbol{n}$ denotes the unit normal vector on all crack surface S in the volume of a representative element V_e.

Costin [77] employed a damage mechanics approach, in which the evolution equation of a damage parameter is derived on the basis of fracture mechanics analysis of a single isolated tensile crack. Besides the stress-induced crack growth, time-dependent crack growth due to stress corrosion cracking is also considered.

Recently, Nemat-Nasser and Obata [78] used an approximate but simple closed-form expression for the response of the sliding crack proposed by Horii and Nemat-Nasser [68] to reproduce stress–strain curves

Table 1. Summary of proposed continuum models for rocks under compression and employed micromechanical models.

Reference	Micromechanical model	Note
Moss and Gupta [74]	sliding crack, elliptic crack	pseudo 3D
Kachanov [75, 76]	tension and sliding penny shape crack	3D
Costin [77]	tensile crack	3D
Nemat-Nasser and Obata [78]	sliding crack	2D, including unloading regime
Okui and Horii [79, 80]	simplified sliding crack	2D, crack interaction
Basista and Gross [81]	sliding crack	2D, based on thermodynamics

of granite under compression for loading as well as unloading paths.

Although these models succeeded in reproducing stress–strain curves of brittle rock up to the vicinity of the peak stress, they can simulate neither the process of microcracking localization nor subsequent macroscopic failure. To predict the macroscopic failure, it is necessary to take account of crack–crack interaction effects.

Okui et al. [79] have proposed a continuum theory which can reproduce localization phenomena, such as axial splitting and shear faulting in brittle rocks. In general, the macroscopic constitutive model based on micromechanics consists of an evolution equation of microdefects and the overall stress–strain relationship for solid with microdefects. In their model, the interaction effects are taken into account in the evolution equation. The strength for macroscopic failure is obtained as an applied stress at a bifurcation point of solution paths. Furthermore, Okui and Horii [80, 82] extended their model to include a time-dependent crack growth mechanism. The validity of the proposed model was examined by comparing its predictions of short-term strength and creep behavior with reported experimental data.

Finally, Basista and Gross [81] formulated a two-dimensional damage model for brittle materials under compression on the basis of Rice's internal variable thermodynamic theory [83]. They derived the macroscopic stress–strain relationship by using Rice's micro-to-macro transition instead of Eq. (6). Employing the sliding crack model, they compared the derived constitutive model with that of Nemat-Nasser and Obata [78] using Eq. (6) to examine the applicability of Rice's theory to constitutive modeling. It was shown that the constitutive model based on Rice's theory is almost identical with the micromechanics-based one. This work demonstrates the new potential of micromechanics as a tool to examine the validity of thermodynamics theories.

7. CLOSURE

The application of micromechanics to modeling rock failure has been reviewed. To encourage new researchers to join this subject, the macroscopic as well as microscopic behavior of rock under compression observed in experiments has been introduced. Attention has been limited to quasi-static behavior of hard rock.

Over the last two decades, developments in microscopic observation and micromechanics in the field of rock mechanics have expounded the fundamental mechanisms of rock behavior, such as axial splitting, shear faulting, the brittle-ductile transition, and so on. Micromechanics has considerable power to explain the mechanisms, which cannot be seen in the phenomenological approach. Micromechanics-based constitutive models have succeeded in reproducing the actual stress-strain relationship quantitatively. Furthermore, some micromechanics-based continuum theories that take the crack interaction into consideration have been able to predict the process of microcrack localization and subsequent macroscopic fracture.

The development of micromechanics in this field has been highly satisfactory, but there remains a lot to do. For example, to take into consideration the interaction effects, a simplified micromechanical model is preferable, while the constitutive model derived from the simplified micromechanical model is prone to be less accurate quantitatively. In fact, there is no fully 3D micromechanics-based continuum theory for rock under compression that takes into consideration the interaction effects. Different routes for formulation of continuum theories based on thermodynamics should also be explored. Dynamic problems, fatigue of rocks, and coupling problems between pore fluid and host rock will be of future interest.

REFERENCES

1. V.S. Vutukuri, R.D. Lama and S.S. Saluja, Handbook on Mechanical Properties of Rocks, **I**, Trans Tech Publications (1974).
2. J. Handin and R. V. Hager, Bull. Am. Assoc. Petrol. Geologists, **41** (1957) 1.
3. W. F. Brace, J. Geophys. Res., **70** (1965) 391.
4. W. F. Brace, B. W. Paulding and C. Scholz, J. Geophys. Res., **71** (1966) 3939.
5. K. Mogi, Rock Mech. Eng. Geology, **4** (1966) 41.
6. W. R. Wawersik and C. Fairhurst, Int. J. Rock Mech. Min. Sci. & Geomech. Abstr., **7** (1970) 561.
7. J. A. Franklin, Rock Mech., **3** (1971) 86.
8. O. Edmond and S. A. F. Murrell, Tectonophysics, **16** (1971) 71.

9. N. Barton, Int. J. Rock Mech. Min. Sci. & Geomech. Abstr., **13** (1976) 255.
10. T. N. Gowd and F. Rummel, Int. J. Rock Mech. Min. Sci. & Geomech. Abstr., **17** (1980) 225.
11. F. Donath, R. T. Faill and D. Tobin, Geol. Soc. Am. Bull., **82** (1971) 1441.
12. H.P. Chin and J.D. Rogers, Rock Mech. and Rock Eng., **20** (1987) 137.
13. R.D. Lama and V.S. Vutukuri, Handbook on Mechanical Properties of Rocks, **III**, Trans Tech Publications, (1974).
14. N.D. Cristescu and U. Hunsche, Time effects in rock mechanics. John Wiley & Sons (1998).
15. W.R. Wawersik, Proc. of 3rd Cong. ISRM, (1974).
16. D.M. Cruden, compression. Int. J. Rock Mech. Min. Sci. & Geomech. Abstr., **11** (1974) 67.
17. L.S. Costin, Fracture Mechanics of Rocks, chapter 5 (ed. by B.K. Atkinson), Academic Press, (1987).
18. D. A. Lockner, J. Geophys. Res., **98** (1993) 475.
19. R.L. Kranz and C. H. Scholz, J. Geophys. Res., **82** (1977) 4893.
20. R.L. Kranz, Int. J. Rock Mech. Min. Sci. & Geomech. Abstr., **16** (1979) 23.
21. R.L. Kranz, J. Geophys. Res., **85** (1980) 1854.
22. J.D. Blacic, J. Geophys. Res., **98** (1993) 15909.
23. E.Z. Lajtai, R.H. Schmidtke and L.P. Bielus, Int. J. Rock Mech. Min. Sci. & Geomech. Abstr., **24** (1987) 247.
24. R.L. Kranz, Tectonophysics, **100** (1983) 449.
25. Z.T. Bieniawski, Int. J. Rock Mech. Min. Sci. & Geomech. Abstr., **4** (1967) 407.
26. M. Friedman, R.D. Perkins and S.J. Green, Int. J. Rock. Mech. Min. Sci., **7** (1979) 297.
27. W.R. Wawersik and W.F. Brace, Rock Mech., **3** (1971) 61.
28. D.K. Hallbauer, H. Wagner and N.G.W. Cook, Int. J. Rock Mech. Min. Sci. & Geomech. Abstr., **10** (1973) 713.
29. S. Mosher, R.L. Berger and D.E. Anderson, Rock Mech., **7** (1975) 167.
30. A. Timur, W.B. Hempkins and R.M. Weinbrandt, J. Geophys. Res., **76** (1971) 4932.
31. P. Tapponnier and W. F. Brace, Int. J. Rock Mech. Min. Sci. & Geomech. Abstr., **13** (1976) 103.
32. E.S. Sprunt and W.F. Brace, Int. J. Rock Mech. Min. Sci. & Geomech. Abstr., **11** (1974) 139.
33. K. Hadley, J. Geophys. Res., **81** (1975) 3484.
34. R.L. Kranz, Int. J. Rock Mech. Min. Sci. & Geomech. Abstr., **16** (1979) 37.
35. D.A. Lockner, D.E. Moore and Z. Reches, Proc. 33rd U.S. Symp. Rock Mech., (1992) 807.
36. F.T. Wu and L. Thomsen, Int. J. Rock Mech. Min. Sci. & Geomech. Abstr., **12** (1975) 167.
37. D.A. Lockner and J. Byerlee, Bull. Seis. Soc. Am., **67** (1977) 247.
38. M. Shimada, A. Cho and H. Yukutake, Tectonophysics, **96** (1983) 159.
39. D.A. Lockner, Int. J. Rock Mech. Min. Sci. & Geomech. Abstr., **30** (1993) 883.
40. T. Yanagidani, S. Ehara, O. Nishizawa, K. Kusunose and M. Terada, J. Geophys. Res., **90** (1985) 6840.
41. D.A. Lockner, J.D. Byerlee and V. Kuksenko, Nature, **350** (1991) 39.
42. D.A. Lockner, J.D. Byerlee, V. Kuksenko, A. Ponomarev and A. Sidrin, Observations of quasistatic fault growth from acoustic emission, **96**, Academic Press, London, (1992) 3.
43. D.E. Moore and D.A. Lockner, J. Struct. Geol., **17** (1995) 95.
44. M. Osada, M. Kashino, T. Yamabe and R. Yoshinaka, J. Japan Soc. Eng. Geol., **40** (1999) 36 (in Japanese).
45. M. Osada, T. Yamabe, and R. Yoshinaka, J. Japan Soc. Eng. Geol., **39** (1999) 500 (in Japanese).
46. Y. Zhao, J. Huang, and R. Wang, Int. J. Rock Mech. Min. Sci. & Geomech. Abstr., **30** (1993) 643.
47. G. Hirth and J. Tullis, J. Geophys. Res., **99** (1994) 11731 .
48. H. Kawakata, A. Cho, T. Yanagidani and M. Shimada. Int. J. Rock Mech. Min. Sci. & Geomech. Abstr., **34** (1997) paper No.151.
49. H. Yukutake, J. Geophys. Res., **94** (1989).
50. B.K. Atkinson, Fracture mechanics of rocks, chapter 1 (ed. by B.K. Atkinson) Academic Press, (1987).
51. H. Lian-an and W. Sijing, Int. J. Rock Mech. Min. Sci. & Geomech. Abstr., **22** (1985).
52. B.K. Atkinson and P.G. Meredith, Fracture mechanics of rocks, chapter 11 (ed. by B.K. Atkinson) Academic Press, (1987).
53. Int. Soc. Rock Mech., Int. J. Rock Mech. Min. Sci. & Geomech. Abstr., **25** (1988) 71.
54. R.J. Martin and W.B. Durham, J. Geophys. Res., **80** (1975) 4837.
55. B.J.S. Wilkins, Int. J. Rock Mech. Min. Sci. & Geomech. Abstr., **17** (1980) 365.
56. S.W. Freiman, J. Geophys. Res., **89** (1984) 4072.
57. B.K. Atkinson and P.G. Meredith, Tectonophysics, **77** (1981) 1.
58. P.L. Swanson, J. Geophys. Res., **89** (1984) 4137.
59. B.K. Atkinson, J. Geophys. Res., **89** (1984) 4077.
60. B.K. Atkinson and P.G. Meredith, Fracture mechanics of rocks, chapter 4 (ed. by B.K. Atkinson), Academic Press, (1987).
61. P.G. Meredith and B.K. Atkinson, Phys. of Earth and Planetary Interiors, **39** (1985) 33.
62. R.G. Hoagland, G.T. Hahn and A.R. Rosenfield, Rock Mech., **5** (1973) 77.
63. J.R. Rice, J. Appl. Mech. ASME, **35** (1968) 379.
64. W.F. Brace and E.G. Bombolakis, J. Geophys. Res., **68** (1963) 3709.
65. S. Nemat-Nasser and H. Horii, J. Geophys. Res., **87** (1982) 6805.
66. H. Horii and S. Nemat-Nasser, J. Geophys. Res., **90** (1985) 3105.
67. H. Horii and S. Nemat-Nasser, Int. J. Solids Struct., **21** (1985) 731.
68. H. Horii and S. Nemat-Nasser, Phil. Trans. R. Soc. Lond., **A319** (1986) 337.
69. M.F. Ashby and C.G. Sammis, Pure Appl. Geophys., **133** (1990) 489.
70. M.F. Ashby, S.D. Hallam and née Cooksley, Acta

Metall, **34** (1986) 497.
71. M. Kachanov, Advances in Appl. Mech., Academic press, (1994) 259.
72. S. Nemat-Nasser and M. Hori, Micromechanics: overall properties of heterogeneous materials, North-Holland, (1993).
73. D. Krajcinovic, Mech. Mater., **8** (1989) 117.
74. W.C. Moss and Y.M. Gupta, J. Geophys. Res., **87** (1982) 2985.
75. M. Kachanov, Mech. Mater., **1** (1982) 19.
76. M. Kachanov, Mech. Mater., **1** (1982), 29.
77. L.S. Costin, J. Geophys. Res., **88** (1983) 9485.
78. S. Nemat-Nasser and M. Obata, J. of Appl. Mech., **55** (1988) 24.
79. Y. Okui, H. Horii, and N. Akiyama, Int. J. Eng. Sci., **31** (1993) 735.
80. Y. Okui and H. Horii, J. Geophys. Res., **102** (1997) 14869.
81. M. Basista and D. Gross, Int. J. Solids and Struct., **35** (1998) 487.
82. Y. Okui and H. Horii, Proc. 4th Int. Workshop Localization and Bifurcation Theory for Soils and Rocks, (ed. by Adachi, Oka and Yashima), A.A.Balkema, (1998) 143.
83. J.R. Rice, J. Mech. Phys. Solids., **19** (1971) 433.